Calcite dissolution kinetics at the sediment-water interface in natural seawater.

Olivier Sulpis[1], Claire Lix[1], Alfonso Mucci[1] and Bernard P. Boudreau[2]

[1]GEOTOP and Department of Earth and Planetary Sciences, McGill University, 3450 University Street, Montreal, QC H3A 0E8, Canada

[2]Department of Oceanography, Dalhousie University, 1355 Oxford Street, Halifax, NS B3H 4J1, Canada

Published in Marine Chemistry:

SULPIS O., LIX C., MUCCI A. and BOUDREAU B.P. (2017) Calcite dissolution kinetics at the sediment-water interface in natural seawater. Marine Chemistry **195:** 70-83. http://dx.doi.org/10.1016/j.marchem.2017.06.005.

ABSTRACT

The absorption, or uptake, of anthropogenic CO_2 by the oceans results in a decrease in pH and carbonate ion concentration, $[CO_3^{2-}]$; as a consequence, the saturation state of seawater with respect to $CaCO_3$ minerals (calcite, aragonite) falls, leading to a shallowing of their saturation depths and triggering an increase in their dissolution at the seafloor. Nearly one-third of the seafloor is covered by $CaCO_3$-rich sediments, and their dissolution is the ultimate sink of anthropogenic CO_2. Despite numerous past studies, the kinetics of $CaCO_3$ dissolution in seawater are still poorly quantified, and the mechanisms controlling the reaction are scarcely understood. Results from *in situ* studies disagree with laboratory studies, most of which have been carried out under conditions, e.g., mineral suspensions, that are not representative of processes at the seafloor. Herein we report measurements of the dissolution rate of calcite, formed into synthetic sediment disks by mixing various amounts of this mineral with montmorillonite. These disks were placed in a stirred-flow reactor and exposed to a range of saturation states and shear stress conditions to simulate conditions encountered at the seafloor. The dissolution rates, normalized to the interfacial area of the sediment disks, were linearly dependent on the undersaturation state of the bulk seawater in the reactor; in addition, the rate displayed a square-root dependence on the calcite content under quiescent conditions. The rate of release of reaction products from the sediment increased with stirring rate, i.e., shear stress, until it became invariant at higher stirring rates. This latter result argues that calcite dissolution at the seafloor is transport (water-side) controlled at the shear stresses known to exist at the seafloor, which advises a simpler kinetic description of calcite dissolution at the seafloor.

Keywords: Calcite dissolution; Kinetics; Sediment-water interface; Ocean floor; Acidification; Benthic boundary layer.

1. INTRODUCTION

In 2014, the global atmospheric CO_2 concentration first reached 400 ppm (Tans and Keeling, 2016), exceeding any recorded level for at least the past 800,000 years (Lüthi et al., 2008). Between 1959 and 2008, atmospheric CO_2 concentrations increased at only 43% of the rate of fossil fuel emissions, the rest being either dissolved in the oceans or taken up by the terrestrial reservoir (Le Quéré et al., 2009). The ocean is the largest reservoir of carbon dioxide on Earth and, thus, the largest sink for anthropogenic CO_2 (Gehlen et al., 2007). Consequently, oceanic uptake plays a major role in the regulation of the atmospheric CO_2 budget, mitigating climate change. From 2000 to 2008, it is estimated that about 26% of the anthropogenic CO_2 emitted to the atmosphere was absorbed by the ocean (Gattuso and Hansson, 2011; Sabine and Feely, 2007).

One of the consequences of massive CO_2 dissolution in the ocean is ocean acidification. Absorbed anthropogenic CO_2 is lowering surface ocean water pH. Caldeira and Wickett (2003) predict that, within the next centuries, the pH change may be larger than any inferred from the geological record of the past 300 Myr, excluding changes resulting from extreme/catastrophic events, such as impacts of celestial objects or massive methane hydrate degassing, e.g., Paleocene-Eocene Thermal Maximum; Zachos et al. (2005). Anthropogenic ocean acidification will perturb the oceanic $CaCO_3$ cycle, impeding biogenic calcification and promoting its dissolution (Delille et al., 2005; Feely et al., 2004). The dissolution of $CaCO_3$-rich sediments is the ultimate sink of anthropogenic CO_2 and, if anthropogenic emissions were to cease, would restore the pH of the oceans back to its pre-anthropogenic value on timescales on the order of 10 kyr (Archer, 2005).

The uptake of CO_2 induces $CaCO_3$ dissolution by lowering the carbonate ion concentration, [CO_3^{2-}], and consequently, the saturation state of seawater with respect to calcium carbonate minerals:

$$\Omega = \frac{[\mathbf{Ca^{2+}}][\mathbf{CO_3^{2-}}]}{K_{\mathrm{sp}}{}^*} \qquad (1)$$

where the square brackets indicate total concentrations in mol kg^{-1} of seawater and K_{sp}* is the stoichiometric solubility constant of the mineral of interest (calcite, aragonite, mol^2 kg^{-2} seawater) at the ambient temperature, pressure and salinity (Millero, 1979; Mucci, 1983).

Whereas surface ocean waters are generally supersaturated with respect to calcite and aragonite, cold deep-ocean waters are typically undersaturated with respect to both minerals, mainly because $CaCO_3$ solubility increases with increasing water depth (pressure) (Millero, 1979) and metabolic CO_2 accumulates as deep waters age. The injection of anthropogenic CO_2 to the deep ocean results in a further decrease in CO_3^{2-} ion concentrations, which in turn reduces the saturation state of seawater (equation 1) and raises the depth at which the waters become undersaturated. When overlying waters are undersaturated, biogenic aragonite or calcite settling to the seafloor can dissolve. The degree of undersaturation ($1 - \mathbf{\Omega}$) with respect to each mineral is the driving force behind this dissolution.

$CaCO_3$-rich sediments (>30 wt%), which cover nearly a third of the ocean floor, will ultimately serve to neutralize a large part of the anthropogenic CO_2 delivered to the deep-ocean according to the overall reaction (Archer et al., 1998),

$$CaCO_3 + CO_{2\,(aq)} + 2H_2O \leftrightarrow 2HCO_3^- + Ca^{2+} \qquad (2)$$

The time required for neutralization of the anthropogenic CO_2 is dependent on the CO_2 transfer rate from the surface ocean to the deep ocean, as well as benthic $CaCO_3$ dissolution kinetics (Boudreau, 2013; Caldeira and Wickett, 2003; Tyrrell, 2011).

The kinetics of calcite dissolution are often expressed by a simple empirical equation of the form:

$$r = k(1 - \Omega_c)^n \tag{3}$$

where r is the dissolution rate normalized to the mass (mol g^{-1} yr^{-1}) or surface area (mol m^{-2} yr^{-1}) of the mineral, k is the dissolution rate constant (mol g^{-1} yr^{-1} or mol m^{-2} yr^{-1}), Ω_c is the saturation state of the solution with respect to calcite, see Eq. (1), and n is the reaction order.

Rate constants (k) and reaction orders (n) derived from laboratory studies diverge widely. Keir (1980) derived a high reaction order ($n = 4.5$) to represent the dissolution rates of suspended biogenic and synthetic calcites in seawater. Likewise, Walter and Morse (1985) obtained a high order dependence ($n = 3$) from their study of synthetic calcite dissolution rates in seawater. However, several researchers have argued recently that calcite dissolution kinetics is linearly dependent (i.e., $n = 1$) on the seawater undersaturation (Boudreau, 2013; Hales and Emerson, 1997b). First-order calcite dissolution kinetics appear to be more consistent with results of *in situ* studies of $CaCO_3$ dissolution in the deep sea (Hales and Emerson, 1996, 1997a, b), but diagenetic processes, such as metabolic CO_2 production and bioturbation, may significantly influence these *in situ* rate measurements.

Keir (1983) determined the dissolution rate of calcite in a stirred-flow reactor with (non-suspended) beds of synthetic and natural carbonate sediments. Although his calculated reaction order was nearly the same as found with previous kinetic experiments on suspended sediment (Keir, 1980), the dissolution rate constant was approximately two orders of magnitude lower. Keir (1983) proposed that the presence of a diffusive boundary layer (DBL) at the sediment-water interface (SWI) of his samples might explain the discrepancy in the experimental results.

The DBL is defined as a thin layer of fluid between the solid (possibly porous) surface and the bulk solution, within which molecular diffusion dominates over turbulent transport and whose thickness is influenced by the hydrodynamic conditions (Schlichting, 1979). The DBL can behave as a region of mass-transfer resistance and thus may limit the dissolution at the solid-water interface (Boudreau and Guinasso, 1982; Dade, 1993; Jørgensen and Revsbech, 1985; Santschi et al., 1983; Steinberger and Hondzo, 1999).

When dealing with a single crystal or suspended grains, calcite dissolution can be broken up into several processes or steps taking place concurrently near the dissolving mineral grain, as described in Morse and Arvidson (2002). In such a scheme, one or more reactions occur at the grain surface, while reactants and products must be transported to or from the grain surface. The slowest of these steps determines the rate of the overall reaction, giving rise to the concept of transport versus reaction control.

The transport-reaction "geometry" for the sediment disks in our reactor or for sediments at the seafloor is more nuanced than that of a single crystal or grains in suspension, and the concept of control is treated differently (Boudreau and Guinasso, 1982). Whereas the dissolution reaction still occurs at solid surfaces, transport must move reactants within sediment pores and also across a DBL that exists on the water side of the disk or above the sediment-water interface (SWI). The dissolution reaction causes a flux of solute products through both the pores and across the DBL. The question of control shifts from consideration of kinetics of reaction at grain surfaces versus transport of solutes to/away from a crystal/grain to a comparison of rates of processes in the sediment versus transport on the water side of the SWI.

When dissolution of a disk or at seafloor is controlled by rates of the combined reaction and transport within the sediment, then "deep" solute gradients develop within the sediment, on a scale far greater than the thickness on the DBL; the DBL is typically of a thickness of about a millimeter for deep sea conditions, but can be thinner in a reactor. Conversely, under this geometry, transport control refers not to the rate of diffusion (or perhaps advection) of solutes within the sediments, but to the rate of transfer across the DBL (Boudreau and Guinasso, 1982). This particular dichotomy is adopted because control by DBL transport will cause the reaction rate to be affected by benthic currents, whereas control by processes within the sediments will be impervious to such effects (baring resuspension or flow penetration). In this study, we will refer to transport and surface reaction limitations that take place within the sediment as "sediment-side control" and to diffusion limitation through the DBL above the bed as "water-side control". Note that dissolution controlled by water-side processes (DBL transport) are inherently linear, which would stand in contrast to past assertions of high-order nonlinearity for calcite dissolution.

Previous laboratory-based $CaCO_3$ dissolution studies have removed the role of water-side processes by re-suspending the sediment in seawater in order to expose all the mineral surfaces and minimize the boundary layer around each grain (Gehlen et al., 2005; Keir, 1980; Morse, 1978; Walter and Morse, 1985). Although these studies provide good insights on calcite dissolution kinetics in the water column (after normalization to the exposed surface area), they are not representative of benthic dissolution conditions (Boudreau, 2013). Although several research groups have demonstrated that calcite dissolution rates become (classically) transport-controlled for pH < 4 and low saturation states, i.e., $\Omega_c < 0.4$ (Berner and Morse, 1974; Morse and Arvidson, 2002; Sjöberg and Rickard, 1984), these conditions diverge widely from those encountered at the seafloor. In this study, we investigated the dissolution kinetics of a simulated organic-free carbonate-rich sediment in natural seawater held in a thermostated, stirred-flow reactor over a range of undersaturations in an attempt to simulate conditions more representative of the seafloor.

2. MATERIALS AND METHODS

2.1. SEAWATER AND SEDIMENT PREPARATION

The natural seawater used for our experiments was collected between 2013 and 2016 at 300 to 400 meters depth in the Gulf of St. Lawrence and stored in high-density polyethylene (HDPE) carboys. These waters originate from the northwestern Atlantic Ocean (Koutitonsky and Bugden, 1991). The practical salinities (S_P) of the seawater were between 34.55 and 34.79 at the time of sampling, as determined by the Seabird SBE-911 conductivity probe mounted on the sampling rosette. Aliquots stored in glass bottles revealed that the soluble reactive phosphate (SRP) concentrations at the time of sampling were between 1.94 and 2.24 µM, whereas dissolved organic carbon (DOC) concentrations were between 53 and 67 µM (Y. Gélinas, pers. comm.). Prior to use, the seawater was pre-equilibrated for several days in the presence of calcite powder (solid:solution ratio of 15g:1L) to scavenge SRP and DOC, both strong calcite dissolution and precipitation inhibitors (Berner and Morse, 1974; Sjöberg, 1978), by adsorption onto the mineral surface. The slurry was then vacuum-filtered through a 0.45 µm Millipore polycarbonate filter and the seawater stored in Nalgene low-density or high-density polyethylene (LDPE or HDPE) bottles for several months. After that period, the SRP concentrations were between 1.48 and 1.67 µM.

ACS reagent grade $CaCO_3$ powder was purchased from Baker® and an XRD analysis confirmed that it was pure calcite, although trace amounts of other polymorphs would have gone undetected if present at less than a few weight percent. The average length of the grains was estimated at 5.65 ± 0.92 µm from a sample of 150 grains examined in a scanning electron microscope (SEM). Based on the latter, and assuming that the shape of the grains is cubic, the geometric specific surface area of the calcite was estimated at 0.39 ± 0.23 m^2 g^{-1}. The calcite powder and the rhombohedral shape of the grains can be seen in Fig. 1.

A highly purified montmorillonite clay (Mineral Colloid® BP) with specific gravity of 2.6 g cm^{-3}, purchased from Southern Clay Products Inc. USA, was used to make the simulated carbonate-rich sediment. The montmorillonite-calcite mixture was prepared by mixing 35 g of montmorillonite and 40 g of calcite powder (53 wt% calcite) into 100 mL of seawater under constant stirring and the homogeneous mixture laid out in the cut-out bottom of LDPE bottles to form uniform disks of various thicknesses and diameters. Disks containing 10, 30, 90 and 100 wt% calcite on a dry basis were also prepared following the same procedure. The main criteria used to assess the suitability of the synthetic sediment was the cohesion and stability of the mixture, especially at the sediment-seawater interface when the beaker was jiggled. The fresh disks were stored in calcite-equilibrated seawater and kept in the dark to avoid the proliferation of bacteria until used within a few days. Based on weight loss upon drying at low temperature (<50°C), an average solid density of 2.65 (from 2.61 for a sediment with 10 wt% of calcite to 2.71 for pure calcite), and the salinity of the seawater, the primary porosity (Φ) of the simulated 53 wt% of calcite sediment was estimated at 0.79 ± 0.01 (n = 5). Given the similar specific gravity of the calcite and montmorillonite powders (respectively 2.71 and 2.6 g cm^{-3}), the sediment disks porosity was, within the uncertainty of our determinations, independent of the calcite content. Freeze-drying of the wet 53 wt% of calcite sediment yielded a similar primary porosity of 0.801 ± 0.002 (n = 4).

Dissolution experiments were also performed on cylindrical cores (4.9 to 7.2 cm in diameter, 3.5 to 6.5 cm thick) of Indiana limestone (see ILI (2007)) inserted tightly into the cut-out bottom of LDPE bottles so that only the flat surface of the disk was exposed to the solution. The limestone porosity was estimated at 0.144 using the Mercury Intrusion Porosimetry (MIP) technique (P. Selvadurai, pers. comm.). The grain size of Indiana limestone is usually quite variable, ranging from < 5 μm to > 300 μm and its macropores (i.e., features with diameter > 33 μm) are not interconnected (i.e., isolated; Ji et al. (2012)). Assuming that only the surface of the Indiana limestone is dissolving, it is possible to observe the dependence of the measured alkalinity flux on the stirring rate due to the diffusion through the DBL, regardless of potential variations of the diffusion depth, i.e., the maximum sediment depth over which the reactants and reaction products diffuse within the sediment.

2.2. STIRRED-FLOW REACTOR

The experimental design depicted in Fig. 2 is based on the principle of the stirred-flow reactor (Denbigh, 1944; Keir, 1980, 1983). Dissolution experiments were carried out in a water-jacketed reaction vessel held at 25.0 (± 0.1) °C and in which the synthetic sediment, including its LDPE mold, was immersed. Between 175 and 872 mL of the treated natural seawater (depending on the volume of the reactor and thickness of the sediment disk) were added to the reactor without disturbing the sediment surface.

The calcite contained in the synthetic sediment, if exposed to a solution undersaturated with respect to calcite ($\Omega_c < 1$), will normally dissolve. In order to obtain an undersaturated solution, a fraction of the treated seawater was acidified by adding dilute hydrochloric acid (~1N) to reduce the total alkalinity (TA) from ~2300 μmol kg^{-1} to ~400 μmol kg^{-1} ("TA in" in Tables 1 and 2) and Ω_c from ~4 to ~0.15. This treatment did not modify the original salinity of the seawater by more than 0.2% (relative). The acidified seawater was equilibrated with the ambient atmosphere ($p\mathrm{CO}_2 \sim 400$ ppm) by bubbling laboratory air with an aquaria pump at a constant flow rate of ~1 mL s^{-1}. The air was pre-humidified, by bubbling it through a distilled water-filled, glass-washing bottle equipped with a fritted disk, to avoid evaporation and salinity variations of the seawater solutions. At room temperature (23 ± 1°C), it took approximately 24 hours to equilibrate the solutions with the atmosphere, as determined from measurements of the $\mathrm{pH_T}$ (pH on the total hydrogen ion scale) and TA of the solution. This acidified seawater served as the input solution and was injected into the reactor at a constant rate through a 0.51 mm inner diameter (ID) Tygon polyvinylchloride (PVC) tube, using a multi-channel peristaltic pump (Gilson's Minipuls$^{\mathrm{TM}}$ 3 Peristaltic Pump). The pumping rate was determined for each setting in each experiment by weighing the amount of solution pumped out of the reactor over a fixed period of time. To keep a constant volume of solution in the reactor, the solution was withdrawn from the reactor by the same pump through a 0.76 mm ID tube fixed at the surface of the solution. The batch reactor was capped by a PVC cover equipped with multiple openings for insertion of the stirrer, the solution input and output tubes, and a combination glass-reference pH electrode. The outer shell of the reactors was wrapped in opaque paper to avoid the proliferation of bacteria that otherwise developed within a few weeks. A stirrer, whose design was inspired by the shear stress inducer described by Javadi and Khalili (2009), was used and driven by an overhead, variable-speed motor. In theory, the stirrer is designed to generate a uniform, bottom shear stress and consists of a rotating 3.5 cm diameter PVC cone held at the tip of a 13 cm long PVC shaft (Fig. 2). The diameter of the stirrer (3.5 cm) was, depending on the diameter of the reactor (between 6.5 and 8.5 cm), between 54 and 41% of the latter, respectively.

The evolution of the dissolution reaction was assessed by monitoring the pH_T of the experimental solution inside the reactor at a fixed acidified seawater pumping rate. Once a steady-state pH_T was achieved, an aliquot of the output solution was collected and analyzed to determine the steady-state TA, S_P and SRP concentration. The pumping rate was then increased and, consequently, the residence time of the solution in the reactor as well as the saturation state of the reactor solution decreased, triggering an increase of the calcite dissolution rate. Residence times of the input solution in the reactors varied between 8.2 and 603.1 hours, corresponding to input flow rates between 0.4 and 72.2 g hr^{-1}, respectively. The experiments were carried out over several weeks or months depending on the injection rate and the range of saturation states investigated. The sediment disks were replaced after no more than two months. Note that, in our experimental design, the saturation state of the bulk solution was not fixed and reached a steady state upon balancing the pumping rate of acidified seawater and calcite dissolution rate.

2.3. ANALYTICAL METHODS

pH_T was measured inside the reactor with a Radiometer Analytical® GK2401C combination glass electrode connected to a Radiometer Analytical® PHM84 pH/millivolt-meter. Prior to each measurement, the electrode was calibrated against three NIST-traceable buffer solutions: pH-4.00, pH-7.00 and pH-10.00 at 25°C. The pH values of these low ionic strength buffers are assigned under the infinite dilution convention. The electrode response to these buffers was then least-squares fitted to obtain the Nernstian slope and measurements converted to the "total" hydrogen ion concentration scale (pH_T), defined under the constant ionic medium convention (Dickson, 1984), using a TRIS buffer solution with an assigned pH_T of 8.089 at S_P = 35 and 25°C.

TA was determined by potentiometric titration of the initial reservoir and steady-state solutions with a dilute hydrochloric acid solution (0.01N), using an automated Radiometer (TitraLab865®) titrator and a Red Rod® combination pH electrode (pHC2001). The dilute HCl titrant was calibrated prior, during, and after each titration session, using certified reference materials (CRM Batch #131 and #140) provided by Andrew Dickson (Scripps Institute of Oceanography) and a laboratory sub-standard of Lower St. Lawrence Estuary seawater (S_P = 34.41; TA = 2283 ± 3 μmol kg^{-1}). The reproducibility of the method was better than 0.5%. The uncertainties presented in this study for total alkalinity, as well as steady-state pH_T, were estimated based on multiple replicate measurements of each sample.

The change in calcium concentration brought by the dissolution of calcite was computed from the difference in TA between the input ("TA in") and the output ("TA out") solutions.

$$\Delta[\mathrm{Ca}^{2+}] = \frac{\Delta\mathrm{TA}}{2} \tag{4}$$

The salinity of the experimental solution was monitored regularly by potentiometric titration of an aliquot of the output solution with a $AgNO_3$ solution calibrated with IAPSO standard seawater. The measurements were performed with an automated Radiometer (TTT80) titrator, a silver electrode, and a mercuric sulfate reference electrode. The reproducibility was better than 0.2%.

The SRP concentration of the initial reservoir and steady-state solutions was determined spectrophotometrically using the technique developed by Murphy and Riley (1962) and described in Grasshoff et al. (1999). The absorbance of the phosphomolybdate reaction product was measured manually at 880 nm on a Hewlett-Packard Agilent 8453 UV-visible spectrophotometer using a 10-cm cell. The detection limit was 0.01 μM and the reproducibility was better than 0.5%. Calibration curves were constructed by 4 successive dilutions of a 10 mM standard phosphate stock solution in a 0.7M NaCl solution to prevent salt effects and the corresponding R^2 values were always better than 0.999.

2.4. CARBONATE SYSTEM CALCULATIONS

At a given temperature, salinity and pressure, only two of the following four measurable carbonate-system parameters, i.e., TA, pH, pCO_2 and DIC, and the appropriate carbonic acid and boric acid dissociation constants are sufficient to estimate the speciation of dissolved inorganic carbon in solution. The Microsoft Excel version of CO2SYS (Pierrot et al., 2006), based on the original algorithm of Lewis and Wallace (1998), was used to calculate the initial reservoir and steady-state solution pCO_2, carbonate ion concentration and saturation state with respect to calcite (Ω_c) from the steady-state pH_T and TA. The uncertainties on Ω_c values reported in Tables 1 and 2 were computed separately and included errors on the solubility constant. All calculations were carried out on the total hydrogen ion concentration scale, using the stoichiometric carbonic acid dissociation constants determined by Lueker et al. (2000), as recommended by Dickson et al. (2007) (see Orr et al. (2015)), the total boron concentration $[B]_T$ value from Uppström (1974), and the standard acidity constant of the HSO_4^- ion ($K(HSO_4)$) from Dickson (1990). The SRP, S_P, T, TA and pH_T were used as input parameters in CO2SYS.

2.5. *DISSOLUTION RATE ESTIMATES*

The calcite dissolution rate r (mol m^{-2} yr^{-1}) was determined from the difference in the composition of the input and output solutions (ΔTA/2 or Δ[Ca]), according to:

$$r = \frac{m_{\mathrm{SW}}\,\Delta\mathrm{TA}}{2\,S\,\Delta t} \tag{5}$$

where m_{SW} is the mass of seawater present in the reactor, Δt is the residence time of the solution in the reactor (yr), as given by the volume of solution in the reactor divided by the pumping rate, and S is the surface area of the simulated sediment disk (interface surface area; ISA).

Dissolution experiments were carried out over a range of undersaturations representative of deep-sea conditions, i.e., Ω_c between 1.0 and 0.6 (Dunne et al., 2012), and a few data points were obtained at higher degrees of undersaturation ($\Omega_c \sim 0.4$). The data were fitted to the logarithmic form of Eq. (3) (i.e., $\log(r)$ vs $\log(1-\Omega_c)$) to estimate the dissolution rate constant (intercept) and the reaction order (slope). Given the nearly invariant calcium concentration in the deep ocean (and our reactors), the degree of undersaturation, $(1-\Omega_c)$, can also be expressed as a difference between the carbonate ion concentration at equilibrium with $CaCO_3$, C_S, and the carbonate concentration in the overlying water, C_0 (Boudreau, 2013; Boudreau and Guinasso, 1982). Under this formalism, the dissolution rate, r, is related to the product of concentration difference, $(C_S - C_0)$, and an overall (or apparent) mass-transfer coefficient for the dissolved CO_3^{2-}, here referred to as k^*. As explained in Boudreau and Guinasso (1982), for linear dissolution kinetics, k^* has units of length per unit time and is a non-linear combination of both the sediment-side mass transfer coefficient (k_S) and the water-side mass transfer coefficient, β, calculated as the CO_3^{2-} diffusion coefficient divided by the thickness of the DBL (Boudreau, 2013), i.e.,

$$k^* = \frac{k_S\,\beta}{(k_S + \beta)} \tag{6}$$

We chose to use the Williamson-York bivariate iterative fitting method described in Cantrell (2008) and based on the work of Williamson (1968) and York (1969) to fit our data to Eqn. (3). This method accounts for uncertainties in both the dissolution rate (r) and undersaturation state $(1-\Omega_c)$ (or in both k^* and $(C_S - C_0)$, as discussed above), and minimizes the deviation between data points and the fitted line along both axes, rather than a standard least-squares fit that simply considers variations in the y-direction. For each fit, we report both the determination coefficient (R^2) and the goodness of the bivariate fit as defined in York et al. (2004) and Cantrell (2008), its expected value being unity.

2.6. SHEAR STRESS GENERATION

Hydrodynamic conditions at the reactive surface of a non-porous media are commonly represented in the framework of the diffusive boundary layer model (Boudreau and Jørgensen, 2001; Levich, 1962; Santschi et al., 1983; Schink and Guinasso, 1977). As noted above, the thickness of the DBL is influenced by hydrodynamic conditions or shear stress at the solid-solution interface (Schlichting, 1979).

Experimental reactor designs that yield a uniform bottom shear stress have been the subject of numerous studies, but have not been entirely satisfactory (Buchholtz-ten Brink et al., 1989; Khalili et al., 2008). Our shear-stress inducer device presumably generates a quasi-uniform bottom shear stress and consists of a right circular cone (cone radius of 1.75 cm, cone angle of 5°), rotating (stirring speed between 0 and 416 rpm) in a fixed cylindrical container, with a vertical gap between the SWI and the apex of the cone of approximatively 1.5 cm (Javadi and Khalili, 2009; Khalili et al., 2008). The bottom surface shear stress (τ), neglecting the vertical side wall, can be computed from the cone parameters from the equations of Javadi and Khalili (2009). Nevertheless, qualitative observations of the water flow in the reactor using a dye with a density similar to seawater reveal that the shear stress estimates derived from the equations of Javadi and Khalili (2009) underestimate the fluid velocity by at least one order of magnitude under our experimental conditions.

3. RESULTS

Sediment disk descriptions, experimental conditions and dissolution rate measurement results, along with all their relative uncertainties, are reported in Table 1 (sediment disks with 53 wt% calcite at various stirring speeds) and Table 2 (sediment disks of various calcite content in unstirred reactors). Salinity measurements of aliquots of the steady-state output solutions (S_P varied between 34.45 ± 0.04 and 36.88 ± 0.04) revealed that even after two months, evaporation was minimal and all calculations were carried out at the *in situ* salinity. During each phase of the experimental protocol, seawater was nearly in equilibrium with the atmosphere. pCO$_2$'s computed using CO2SYS from the steady-state S_P, TA, pH$_T$ and [SRP] values of samples varied between 344 and 575 ppm.

3.1. *QUIESCENT CONDITIONS*

We ran a number of experiments without stirring (rotation). If these are controlled by diffusion in the water column, then the rate should be linear. A bivariate linear fit to the data, without forcing the intercept through origin (red line in Fig. 3), yields

$$r_0 = (3.5 \pm 1.0\ \mathrm{mol\ m^{-2}\ yr^{-1}})\ (1 - \Omega_c) + (-0.4 \pm 0.4\ \mathrm{mol\ m^{-2}\ yr^{-1}}) \tag{7a}$$

$$r_0 = (102.4 \pm 28.6\ \mathrm{m\ yr^{-1}})\ (C_S - C_0) + (-0.7 \pm 0.5\ \mathrm{mol\ m^{-2}\ yr^{-1}}) \tag{7b}$$

where r_0 is the ISA-normalized dissolution rate under water-side control, where the limiting step is diffusion in the water column. Eq. (7a) reports the dissolution rate law in terms of undersaturation state with respect to calcite and Eq. (7b) is the fit with respect to the deviation of [CO$_3^{2-}$] from equilibrium (C_S – C_0), as explained in Section 2.5. The goodness of the linear fit (Cantrell, 2008; York et al., 2004) was 0.44 for Eq. (7a) and 0.50 for (7b), whereas the R^2 value was estimated to be 0.47 for Eq. (7a) and 0.48 for (7b), which reflect the limited data at our disposal.

Figure 4 is a plot of the calcite dissolution rates as a function of the undersaturation state with respect to calcite, in unstirred reactors for different relative calcite contents. Linear regressions to the rate data for each calcite content were applied to estimate their rate constants as a function of the undersaturation. As indicated in Fig. 5, the ISA-normalized dissolution rate constant determined under quiescent conditions increases slowly with the calcite content and reaches a plateau for the highest calcite contents (90 and 100 wt%). A standard least-squares regression of the calcite dissolution rate constant (k) to the calcite weight fraction in a dry sediment (B) yields a square-root dependence of 0.54 ± 0.17, with a correlation coefficient R^2 = 0.78. This relationship is in excellent agreement with the prediction of Boudreau and Guinasso (1982), Boudreau (2013) and Keir (1982) that, when calcite is the single calcium carbonate mineral present in a sediment, the dissolution rate is proportional to the square root of the reactive surface area, assuming that the reactive surface area of calcite increases linearly with the calcite content.

3.2. *STIRRED CONDITIONS*

In the discussion that follows, we neglect irregularities at the surface of our synthetic sediment disks (millimetre-scale and smaller), assume that a continuous and uniform DBL is present above the SWI (which varied with rotation), which we recognize as inaccurate, and that fluid movement within the pores (< 15 µm) of sediment is through molecular diffusion. In defense of these assumptions, surface irregularities on a scale smaller than the viscous sublayer (about 1 cm in the deep sea) will not seriously affect mass transfer. In addition, the synthetic sediment made with montmorillonite should have permeabilities that are so low as to prevent any appreciable water flow (Boudreau, 1997), and what remains is molecular diffusion.

Figure 6 shows the dependence of the dissolution rates of Indiana limestone on the stirring rate. Interface area-normalized (ISA-normalized) calcite dissolution rates of Indiana limestone disks increased from 1.1 ± 0.1 to 5.4 ± 0.6 mol m^{-2} yr^{-1} as the stirring rate was increased from 0 and 53 rpm and as Ω_c rose from 0.23 ± 0.04 to 0.38 ± 0.03. At higher stirring rates (> 53 rpm), the ISA-normalized rates did not vary significantly, nor did the saturation state of the bulk solution. Thus, we conclude that the Indiana limestone dissolution rate is controlled by mass transport through the DBL above the bed for stirring speeds ≤ 53 rpm. Above this value, the dissolution regime shifts from a water-side transport control to a sediment-side control, when the DBL above the sediment bed has been thinned enough that k_S, the sediment-side control term, becomes smaller than β (see De Baere et al. (2016)), as determined by equation (6).

Results of the calcite dissolution kinetic experiments with sediment disks containing 53 wt% calcite can be regrouped into 4 distinct sets based on the stirring rates investigated: 0, 39, 74 and 96 rpm. Like the Indiana limestone experiments, the ISA-normalized calcite dissolution rate from the sediment disks increased as the stirring rate was increased from 0 and 74 rpm, but, as shown in Fig. 3, became invariant between 74 and 96 rpm. Assuming those results that exhibited stirring-rate dependence were sediment-side (transport) controlled, then the dissolution rate should be linearly proportional to the undersaturation state of seawater with respect to calcite, as implied by Fick's first law of diffusion.

A total of 43 dissolution experiments on sediment disks containing 53 wt% calcite and 16 additional experiments on sediment disks of various calcite content were carried out at 25°C and ambient atmospheric pressure. The dissolution kinetics were investigated over a large range of saturation states with respect to calcite, ranging from highly undersaturated (Ω_c = 0.37 ± 0.02) to slightly supersaturated (Ω_c = 1.05 ± 0.05) solutions. The best fits (black line on Fig. 3) to the experimental dissolution measurements carried out under stirred conditions (39, 74 and 96 rpm) yield:

$$r = (10.8 \pm 1.4\ \mathrm{mol\ m^{-2}\ yr^{-1}})\ (1 - \Omega_c)^{1.27 \pm 0.22} \tag{8a}$$

$$r = (14.3 \pm 1.5\ \mathrm{mol\ m^{-2}\ yr^{-1}})\ (1 - \Omega_c) + (-1.9 \pm 0.5\ \mathrm{mol\ m^{-2}\ yr^{-1}}) \tag{8b}$$

$$r = (326.9 \pm 39.5\ \mathrm{m\ yr^{-1}})\ (C_\mathrm{S} - C_0) + (-1.7 \pm 0.5\ \mathrm{mol\ m^{-2}\ yr^{-1}}) \tag{8c}$$

The goodness of the fit was 1.01 for Eq. (8a), 1.16 for Eq. (8b) and 1.15 for Eq. (8c), whereas the R^2 values were, respectively, 0.51, 0.76 and 0.77; hence, a linear model properly describes the data, and the dissolution kinetics, under our experimental conditions, are well represented by a law that does not go through origin.

The ISA-normalized rate dependence on (1 – Ω_c) is nearly linear, as reported in Eq. (8a). As explained in Boudreau (2013), setting an intercept through the origin introduces a statistically biased restriction, as this intercept is part of the overall experimental uncertainty. As discussed later in this paper, deviations of the intercept from the origin can be explained by the contribution of parallel reactions. The rate constant (*k*) in Eq. (8b) is about 4 times larger than the water-side transport-controlled rate constant from Eq. (7a) determined under quiescent conditions (unstirred reactors). As noted previously, there is no significant variation of the measured dissolution rates at stirring rates between 74 and 96 rpm; consequently, the dissolution rate is believed to be controlled by processes at and below the SWI, i.e., sediment-side control (Boudreau, 2013; Boudreau and Guinasso, 1982) at these stirring rates.

4. DISCUSSION

4.1. LINEAR DISSOLUTION KINETICS

Most laboratory-derived calcite dissolution rate data published to date (Cubillas et al., 2005; Gehlen et al., 2005; Keir, 1980, 1983; Morse, 1978; Subhas et al., 2015; Teng, 2004; Walter and Morse, 1985; Xu et al., 2012) display a non-linear dependence on the saturation state of the solution, regardless of their experimental design or measurement techniques. Conversely, several researchers have attempted to demonstrate a linear relationship between calcite dissolution rate and saturation state in seawater (Boudreau, 2013; Emerson and Bender, 1981; Hales and Emerson, 1997b). Hales and Emerson (1997b) re-evaluated Keir (1980)'s original experimental data for suspended sediment and found evidence that calcite dissolution rates may be linearly correlated to the saturation state of the seawater solution. They reached this conclusion after assuming that the saturation states of the experimental solutions were underestimated, more specifically that the calcite stoichiometric solubility product used to calculate the saturation state was erroneous and overestimated. Likewise, after a re-examination of Keir (1983)'s original experimental data with natural carbonate sediments, Boudreau (2013) concluded that linear $CaCO_3$ dissolution kinetics were inherent to the data, even without having to call upon a revised solubility.

Previous studies have advanced that the calcite dissolution reaction is reaction-controlled near equilibrium, $\Omega \rightarrow 1$, and tends to be transport-controlled far from equilibrium, $\Omega << 1$, e.g., (Morse and Arvidson, 2002; Sjöberg and Rickard, 1984). We have found that calcite dissolution rates (Figs 3 and 4) are linear, regardless of the controlling regime (water-side versus sediment-side), which contradicts the conclusions of these past studies. Furthermore, the observed dependence of the rate on stirring below 74 rpm indicates sediment-side control for hydrodynamic conditions below this stirring limit, regardless of the degree of undersaturation, a point that also contradicts past conclusions. Whereas it is difficult to translate our stirring rates to oceanic conditions, we firmly believe that the fit that we report based on linear relationships between the dissolution rate and the undersaturation state are more representative of the processes occurring at the seafloor. Simple dye tracer experiments in our experimental vessels (not shown) reveal that water velocities are much faster at all our stirring rates than velocities estimated for the deep sea, i.e., between 0.1 and 1 cm s^{-1} (Dade, 1993).

All our linear fits contain a positive intercept on the x-axis, i.e., over-estimated undersaturation, and thus a negative y-axis intercept i.e., a lower than expected rate error (see Figs 3 and 4). Two explanations for lower apparent solubility on the time scales of our experiment come to mind. One could be elevated pore-water SRP concentrations. SRP is released by desorption from the montmorillonite. SRP is known to be a strong inhibitor of both calcite dissolution and precipitation (Berner and Morse, 1974; Burton and Walter, 1990; Morse, 1974; Mucci, 1986; Sjöberg, 1978) due to its adsorption at high-energy sites on the calcite mineral surface (Alkattan et al., 2002; Millero et al., 2001; Svensson and Dreybrodt, 1992). These past studies have attributed this effect to a lower rate constant for the dissolution reaction, but a lower rate can also be affected by a smaller apparent solubility (on the experimental time scale). Another possibility are effects from the concurrent precipitation of a slightly less soluble form of $CaCO_3$ containing up to 4 mole% $MgCO_3$ (Bischoff et al., 1987), during dissolution.

In situ pore-waters microelectrode profiles of conductivity, oxygen and pH have shown calcite dissolution to occur over the first cm in deep-sea sediments overlain by undersaturated seawater (Archer et al., 1989a; Archer et al., 1989b; Oxburgh and Broecker, 1993), which suggests that dissolution does not occur primarily at the sediment-seawater interface, as implied by our results. Two factors may, however, account for these observations. The first is that real deep-sea sediments contain labile organic matter that is subject to microbial oxidation, which produces CO_2. The metabolic CO_2 can induce $CaCO_3$ dissolution (Emerson and Bender, 1981), and this effect is indicated in the original Keir (1983) results; the latter display dissolution even when the overlying waters are supersaturated with respect to calcite, which can only be due to metabolic forcing, or aragonite dissolution.

The other possibility is that the observed deeper dissolution is partly an artifact of early micro-electrode measurements. Glud et al. (1994) showed that early micro-electrodes, inserted into sediments from the water-side of the SWI, measured deeper O_2 penetration in sediments than electrodes inserted from below and moved upward. The micro-electrodes from the water-side caused overlying water to penetrate the sediment to some extent; if this afflicted the Archer et al. (1989a, 1989b) study, then undersaturated overlying waters may have been introduced into the sediment, leading to dissolution at depths where no dissolution was occurring previous to electrode insertion. Our experiments show that $CaCO_3$ dissolution responds rapidly to changes in saturation state, so that this artifact is a possibility.

Finally, to investigate if a gradient in the calcite content developed within the sediment disks following the dissolution experiments, coulometric measurements were performed on the synthetic sediment disks. The inorganic carbon content of our un-reacted and reacted synthetic sediment disks was determined at ~2 mm resolution (following freezing of the disks and shaving with a scalpel) by coulometry (reproducibility of 0.5%, detection limit of 0.15%). Whereas the calcite content within the un-reacted simulated sediment varied slightly (45.9 ± 0.1% C or 49.2 ± 0.8% $CaCO_3$), no discernable gradient developed within the reacted sediments. This observation might not be surprising because one would not expect a detectable concentration gradient to develop, even if restricted to the top first cm, unless dissolution had been carried out for several months at the lowest undersaturation investigated.

4.2. SEDIMENT-SIDE DISSOLUTION RATE CONSTANTS

Calcite dissolution rate constants determined in the laboratory in seawater can be several orders of magnitude higher than results of *in situ* measurements (Green and Aller, 2001; Hales and Emerson, 1997a). Calcite in deep-sea sediments is mostly biogenic (Honjo et al., 1982; Sun and Turchyn, 2014) and may be less reactive than the reagent-grade calcite used in laboratory studies, although natural calcitic sediments dissolved in laboratory experiments yielded rate constants similar to those of synthetic calcite (Keir, 1980, 1983; Walter and Morse, 1985). It is interesting to note that lower rate constants are consistently determined for biogenic carbonates than for synthetic calcite. This discrepancy has been ascribed to the different approaches used to determine the surface area of the solids and the normalization of the rates (Lüttge, 2005; Lüttge et al., 2013). As noted by Colombani (2016), there is no consensus about the magnitude of the calcite dissolution rate constant due to the extremely diverse conditions under which dissolution experiments have been carried out and the various surface area normalization that have been applied.

The (apparent) sediment-side ISA-normalized rate constant derived from this study (k = 14.3 ± 1.5 mol m^{-2} yr^{-1}) is slightly higher to that obtained from a fit to Keir (1983)'s calcite dissolution experimental results (k_{Keir} = 10.5 ± 1.5 mol m^{-2} yr^{-1}) obtained with pure reagent grade calcite laid down uniformly (~ 0.6 cm thick) at the bottom of a stirred reactor filled with artificial seawater at 20 ± 1°C and atmospheric pressure (Fig. 7). The latter study is, by far, the closest analog to our experiments. Keir (1983) normalized his dissolution rates to the surface area of the reactor bottom, which we denoted as ISA in this study, and gave little information about the hydrodynamic conditions in the reactor. Nevertheless, he noted that the stirring rate was high enough to generate "moderate mixing", but not fast enough to induce resuspension. Based on our results, we believe that his stirring rate was high enough to render the reaction sediment-side controlled, i.e., k_S is the smaller term in the expression of the overall mass transfer coefficient k^*, see Eq. (6).

Our ISA-normalized calcite dissolution rates and those obtained by Keir (1983) with synthetic calcite display notably similar dissolution kinetics (Fig. 7). Boudreau (2013) refitted Keir's data as a function of ($C_S - C_0$) and reported two sediment-side mass transfer coefficients, one for each of the seawater batches used during the dissolution experiments, i.e., 263.1 ± 24.1 and 490.5 ± 89.2 m yr^{-1} for the data Keir (1983) obtained on disks of pure synthetic calcite. These values bracket the sediment-side mass transfer coefficient, i.e., k_S = 326.9 ± 39.5 m yr^{-1} (see Eq. (8c)) that we obtained under similar experimental conditions. The latter observation is interpreted as transport limitation within the sediment, i.e., reaction products accumulate in pore waters and escape the sediment by diffusion, thus constraining the apparent dissolution rate measured at the SWI, in accordance to the square-root dependence of the calcite dissolution rates on the calcite contents of the sediment (Boudreau and Guinasso, 1982) in Fig. 5. Our results are also consistent with Keir's observations that the calcite dissolution rate constant in a sediment increases with its calcite content between 0 and about 60%, whereas it becomes statistically invariant at higher calcite contents (> 60%).

We should note that, on occasion, we measured net $CaCO_3$ dissolution rates (although very weak, see Table 1) at low apparent supersaturations ($\Omega_c \leq 1.05$), as has been reported by Subhas et al. (2015). This may reflect the dissolution of a more soluble $CaCO_3$ polymorph (e.g., XRD- and SEM-undetectable aragonite or vaterite contamination of the reagent grade calcite) or a short-lived surface phase that develops upon the introduction of the pure calcite to the seawater solution, e.g. a magnesian calcite. Mucci and Morse (1983) and Mucci et al. (1985) determined that a 8 mole% magnesian calcite precipitates on pure calcite powders at 25°C from seawater under controlled-laboratory conditions. As this phase is more soluble than pure calcite and the most stable phase in seawater, i.e., minimum solubility at 4 mole% magnesian calcite (Bischoff et al., 1987; Busenberg and Plummer, 1989; Mucci and Morse, 1983), it may lead to an apparent supersaturation. In addition, uncertainties inherent to our saturation state calculations (alkalinity, pH determinations, carbonic and boric acid dissociation constants) also contribute to the apparent supersaturation.

4.3. CALCITE COMPENSATION DEPTH

Whereas calcite dissolves in the oceanic water column below its saturation depth, i.e., the R_0 level or saturation depth where $\Omega_c = 1$ (Ben-Yaakov et al., 1974), it still accumulates in deep-sea sediments down to the calcite compensation depth (CCD). The position of the CCD is determined by the balance between the flux of particulate $CaCO_3$ from the overlying water and the ambient calcite dissolution rate (Berner et al., 1976; Boudreau et al., 2010; Edmond, 1974; Edmond and Gieskes, 1970; Morse and Berner, 1972). In other words, the CCD is the depth below which the seawater undersaturation is sufficient to generate a dissolution rate that is equivalent or faster than burial and the $CaCO_3$ particulate flux (Edmond, 1974).

Assuming an exponential dependence of the calcite solubility on the hydrostatic pressure and linear kinetics, Boudreau et al. (2010) were able to derive a simple expression to estimate the CCD, which can be written, for linear kinetics as:

$$z_{\mathrm{cc}} = \frac{p_{\mathrm{c}}}{\rho\, g} \ln\left(\frac{[\mathrm{Ca}^{2+}]\, F_{\mathrm{B}}}{K_{\mathrm{sp}}{}^{*}\, A_{\mathrm{D}}\, k^{*}} + \frac{[\mathrm{Ca}^{2+}]\, [\mathrm{CO}_3^{2-}]_{\mathrm{D}}}{K_{\mathrm{sp}}{}^{*}}\right) \tag{9}$$

where z_{cc} represents the CCD, p_c is a characteristic pressure set as 511 atm (see Boudreau et al. (2010)), ρ is the mean density of seawater, g is the mean gravitational acceleration on Earth, F_B is the flux of solid calcite from the surface ocean (rain rate), A_D is the seafloor surface below 200 m, and $[CO_3^{2-}]_D$ is the carbonate ion concentration in the deep-ocean.

In order to test this model with our dissolution rate, we must first estimate the overall dissolution mass transfer coefficient (k*) under the hydrodynamic conditions encountered at the seafloor. Dissolution cannot occur faster than the limit placed by transport across the benthic DBL; this transfer limit is embodied by the mass transfer coefficient β. Following the arguments presented in Boudreau (2013), typically β = 12.7 m yr^{-1}, which implies a benthic DBL of about 1.2 mm. The overall mass transfer coefficient computed using Eq. (6) resulting of the benthic estimated β value and the k_S value reported in Eq. (8c) is $k^* = 12.2 \pm 1.5$ m yr^{-1}. Thus, given that our dissolution mass transfer coefficient under sediment-side control is more than 25 times larger than the mass transfer coefficient through the benthic DBL, calcite dissolution at the seafloor is largely controlled by diffusion through the benthic DBL. A similar hypothesis of (at least partial) water-side control on calcite dissolution has previously been considered by several other authors (Broecker, 2009; Oxburgh, 1998; Schink and Guinasso, 1977; Takahashi and Broecker, 1977).

Next, assuming a constant $[CO_3^{2-}]_D$ of 0.09 mM for the average deep ocean (Boudreau et al., 2010; Broecker and Clark, 2003; Key et al., 2004) and a calcite rain rate (F_B) of 40 x10^3 Gmol yr^{-1} (Archer, 1996; Berelson et al., 2007; Sarmiento and Gruber, 2006), we estimate, using Eq. (9), the average calcite compensation depth at 4.4 ± 0.2 km. For a larger calcite export rate (i.e., 60 x10^3 Gmol yr^{-1}), the CCD deepens to 4.6 ± 0.2 km, as compared to a worldwide average of 4.75 km estimated by Boudreau et al. (2010). Note that all our attempts to model the CCD based on non-linear kinetics, using a fit to our data with an order of reaction greater than unity, fail to reproduce the observed world-average CCD. Given a predicted, mean deep-ocean $[CO_3^{2-}]$ of 0.045 mM by the end of this millennia (Ridgwell and Hargreaves, 2007), the CCD would rise to a depth of 1.3 ± 0.2 km for a calcite rain rate of 40 x10^3 Gmol yr^{-1}, regardless of any feedback mechanism in the biological production of calcium carbonate minerals, the climate or the heat content of the ocean (Archer et al., 2009; Ries et al., 2016; Tanhua et al., 2013).

5. CONCLUSIONS

We have measured the dissolution rate of calcite in a synthetic, inorganic sediment when exposed to undersaturated natural seawater and simulated hydrodynamic conditions at the seafloor. Under our experimental conditions, calcite dissolution rates, normalized to the interface area of the sediment surface, vary linearly with the degree of undersaturation of the solution, i.e., $(1 - \Omega_c)$. The dissolution rates of Indiana limestone and the synthetic sediment increase with the stirring rate up to a point where the measured flux of alkalinity becomes independent of the hydrodynamic conditions at the sediment-water interface. The transition corresponds to a shift from a system controlled by water-side transport (across the diffusive boundary layer) to a system controlled by sediment-side processes (reactions within the sediment and diffusion of pore-water solutes), or by surface reactions in the case of Indiana limestone. Furthermore, given that the calcite sediment dissolution rates become square-root dependent on the calcite content at higher concentrations is consistent with the interpretation that rates are controlled by the diffusion and reaction within the sediments at high stirring rates.

Unlike the dissolution kinetic studies carried out during the past decades on carbonate mineral suspensions, our study fills an important knowledge gap by taking into account transport limitations through both the diffusive boundary layer above the sediment bed and the sediment pore waters, and is thus more representative of dissolution occurring at the seafloor. Results of this study are compatible with those of Keir (1983), who used a similar experimental design (sediment disks). A reinterpretation of Keir (1983) by Boudreau (2013) showed that those earlier results also exhibited first-order kinetics and a square-root dependence of the dissolution rate with the calcite content of the sediment. Our sediment-side mass-transfer coefficient ($k_S = 326.5 \pm 35.9$ m yr^{-1}) is more than 25 times larger than the estimated mean water-side mass-transfer coefficient at the seafloor ($\beta = 12.7$ m yr^{-1}), and supports the current paradigm of transport-controlled carbonate dissolution kinetics at the seafloor. Our linear dissolution rate kinetics provide a good prediction of the world-average CCD. Finally, our findings are an important step toward reconciling results of calcite reaction kinetic studies published to date and provide a simplified description of the calcite dissolution kinetics at the sediment-water interface in deep-sea sediment.

Acknowledgements

We wish to thank Constance Guignard for her assistance in the laboratory. This research was funded by a Natural Sciences and Engineering Research Council Discovery grants to A.M. and B.P.B., as well as a MEOPAR grant to A.M. C.L. and O.S. also acknowledge the Dept. of Earth and Planetary Sciences at McGill University for financial support during their residency in the graduate program.

REFERENCES

Alkattan, M., Oelkers, E.H., Dandurand, J.-L. and Schott, J., 2002. An experimental study of calcite dissolution rates at acidic conditions and 25°C in the presence of $NaPO_3$ and $MgCl_2$. Chemical Geology, 190(1-4): 291-302.

Archer, D., 1996. A data-driven model of the global calcite lysocline. Global Biogeochemical Cycles, 10(3): 511-526.

Archer, D., 2005. Fate of fossil fuel CO_2 in geologic time. Journal of Geophysical Research, 110(C09S05).

Archer, D., Eby, M., Brovkin, V., Ridgwell, A., Cao, L., Mikolajewicz, U., Caldeira, K., Matsumoto, K., Munhoven, G., Montenegro, A. and Tokos, K., 2009. Atmospheric Lifetime of Fossil Fuel Carbon Dioxide. Annual Review of Earth and Planetary Sciences, 37(1): 117-134.

Archer, D., Emerson, S. and Reimers, C., 1989a. Dissolution of calcite in deep-sea sediments: pH and O_2 microelectrode results. Geochimica et Cosmochimica Acta, 53(11): 2831-2845.

Archer, D., Emerson, S. and Smith, C.R., 1989b. Direct measurement of the diffusive sublayer at the deep sea floor using oxygen microelectrodes. Nature, 340: 623-626.

Archer, D., Kheshgi, H. and Maier-Reimer, E., 1998. Dynamics of fossil fuel CO_2 neutralization by marine $CaCO_3$. Global Biogeochemical Cycles, 12(2): 259-276.

Berelson, W.M., Balch, W.M., Najjar, R., Feely, R.A., Sabine, C. and Lee, K., 2007. Relating estimates of $CaCO_3$ production, export, and dissolution in the water column to measurements of $CaCO_3$ rain into sediment traps and dissolution on the sea floor: A revised global carbonate budget. Global Biogeochemical Cycles, 21(GB1024).

Ben-Yaakov, S., Ruth, E. and Kaplan, I.R., 1974. Carbonate Compensation Depth: Relation to Carbonate Solubility in Ocean Waters. Science, 184(4140): 982-984.

Berner, R.A., Berner, E.K. and Keir, R.S., 1976. Aragonite dissolution on the Bermuda Pedestal: its depth and geochemical significance. Earth and Planetary Science Letters, 30(2): 169-178.

Berner, R.A. and Morse, J.W., 1974. Dissolution kinetics of calcium carbonate in sea water: IV. Theory of calcite dissolution. American Journal of Science, 274(2): 108-134.

Bischoff, W.D., Mackenzie, F.T. and Bishop, F.C., 1987. Stabilities of synthetic magnesian calcites in aqueous solution: Comparison with biogenic materials. Geochimica et Cosmochimica Acta, 51(6): 1413-1423.

Boudreau, B.P., 1997. Diagenetic Models and Their Implementation. Springer-Verlag, Berlin.

Boudreau, B.P., 2013. Carbonate dissolution rates at the deep ocean floor. Geophysical Research Letters, 40(4): 744-748.

Boudreau, B.P. and Guinasso, N.L., Jr., 1982. The influence of a diffusive boundary layer on accretion, dissolution, and diagenesis at the sea floor. In: K.A. Fanning and F.T. Manheim (Editors), The Dynamic Environment of the Ocean Floor. Lexington Books, Lexington, pp. 115-145.

Boudreau, B.P. and Jørgensen, B.B., 2001. The Benthic Boundary Layer: Transport Processes and Biogeochemistry. Oxford University Press, Oxford.

Boudreau, B.P., Middelburg, J.J. and Meysman, F.J.R., 2010. Carbonate compensation dynamics. Geophysical Research Letters, 37(L03603).

Broecker, W.S., 2009. Wally's Quest to Understand the Ocean's $CaCO_3$ Cycle. Annual Review of Marine Science, 1: 1-18.

Broecker, W.S. and Clark, E., 2003. Pseudo dissolution of marine calcite. Earth and Planetary Science Letters, 208(3-4): 291-296.

Buchholtz-ten Brink, M.R., Gust, G. and Chavis, D., 1989. Calibration and performance of a stirred benthic chamber. Deep Sea Research Part A. Oceanographic Research Papers, 36(7): 1083-1101.

Burton, E.A. and Walter, L.M., 1990. The role of pH in phosphate inhibition of calcite and aragonite precipitation rates in seawater. Geochimica et Cosmochimica Acta, 54(3): 797-808.

Busenberg, E. and Plummer, L., 1989. Thermodynamics of magnesian calcite solid-solutions at 25°C and 1 atm total pressure. Geochimica et Cosmochimica Acta, 53(6): 1189-1208.

Caldeira, K. and Wickett, M.E., 2003. Anthropogenic carbon and ocean pH. Nature, 425(6956): 365-365.

Cantrell, C.A., 2008. Technical Note: Review of methods for linear least-squares fitting of data and application to atmospheric chemistry problems. Atmospheric Chemistry and Physics, 8(17): 5477-5487.

Colombani, J., 2016. The Alkaline Dissolution Rate of Calcite. The Journal of Physical Chemistry Letters, 7(13): 2376-2380.

Cubillas, P., Köhler, S., Prieto, M., Chaïrat, C. and Oelkers, E.H., 2005. Experimental determination of the dissolution rates of calcite, aragonite, and bivalves. Chemical Geology, 216(1-2): 59-77.

Dade, W.B., 1993. Near-bed turbulence and hydrodynamic control of diffusional mass transfer at the sea floor. Limnology and Oceanography, 38(1): 52-69.

De Baere, B., Molins, S., Mayer, K.U. and François, R., 2016. Determination of mineral dissolution regimes using flow-through time-resolved analysis (FT-TRA) and numerical simulation. Chemical Geology, 430: 1-12.

Delille, B., Harlay, J., Zondervan, I., Jacquet, S., Chou, L., Wollast, R., Bellerby, R.G.J., Frankignoulle, M., Borges, A.V., Riebesell, U. and Gattuso, J.-P., 2005. Response of primary production and calcification to changes of $p\mathrm{CO}_2$ during experimental blooms of the coccolithophorid *Emiliania huxleyi*. Global Biogeochemical Cycles, 19(GB2023).

Denbigh, K.G., 1944. Velocity and yield in continuous reaction systems. Transactions of the Faraday Society, 40: 352-373.

Dickson, A.G., 1984. pH scales and proton-transfer reactions in saline media such as sea water. Geochimica et Cosmochimica Acta, 48(11): 2299-2308.

Dickson, A.G., 1990. Standard potential of the reaction: $AgCl(s)+1/2H_2(g) = Ag(s)+HCl(aq)$, and the standard acidity constant of the ion HSO_4^- in synthetic sea water from 273.15 to 318.15 K. The Journal of Chemical Thermodynamics, 22(2): 113-127.

Dickson, A.G., Sabine, C.L. and Christian, J.R., 2007. Guide to best practices for ocean CO_2 measurements. PICES Special Publication 3, 191 pp.

Dunne, J.P., Hales, B. and Toggweiler, J.R., 2012. Global calcite cycling constrained by sediment preservation controls. Global Biogeochemical Cycles, 26(GB3023).

Edmond, J.M., 1974. On the dissolution of carbonate and silicate in the deep ocean. Deep Sea Research, 21: 455-480.

Edmond, J.M. and Gieskes, J.M.T.M., 1970. On the calculation of the degree of saturation of sea water with respect to calcium carbonate under in situ conditions. Deep Sea Research, 34: 1261-1291.

Emerson, S. and Bender, M., 1981. Carbon fluxes at the sediment-water interface of the deep-sea: calcium carbonate preservation. Journal of Marine Research, 39: 139-162.

Feely, R.A., Sabine, C.L., Lee, K., Berelson, W., Kleypas, J., Fabry, V.J. and Millero, F.J., 2004. Impact of Anthropogenic CO_2 on the $CaCO_3$ System in the Oceans. Science, 305(5682): 362-366.

Gattuso, J.-P. and Hansson, L., 2011. Ocean Acidification. Oxford University Press, Oxford.

Gehlen, M., Bassinot, F.C., Chou, L. and McCorkle, D., 2005. Reassessing the dissolution of marine carbonates: II. Reaction kinetics. Deep Sea Research Part I: Oceanographic Research Papers, 52(8): 1461-1476.

Gehlen, M., Gangstø, R., Schneider, B., Bopp, L., Aumont, O. and Ethe, C., 2007. The fate of pelagic $CaCO_3$ production in a high CO_2 ocean: a model study. Biogeosciences, 4(4): 505-519.

Glud, R.N., Gundersen, J.K., Revsbech, N.P. and Jørgensen, B.B., 1994. Effects on the benthic diffusive boundary layer imposed by microelectrodes. Limnology and Oceanography, 39(2): 462-467.

Grasshoff, K., Kremling, K. and Ehrhardt, M., 1999. Methods of Seawater Analysis. Wiley VCH Weinheim, 634 pp.

Green, M.A. and Aller, R.C., 2001. Early diagenesis of calcium carbonate in Long Island Sound sediments: Benthic fluxes of Ca^{2+} and minor elements during seasonal periods of net dissolution. Journal of Marine Research, 59(5): 769-794.

Hales, B. and Emerson, S., 1996. Calcite dissolution in sediments of the Ontong-Java Plateau: In situ measurements of pore water O_2 and pH. Global Biogeochemical Cycles, 10(3): 527-541.

Hales, B. and Emerson, S., 1997a. Calcite dissolution in sediments of the Ceara Rise: In situ measurements of porewater O_2, pH, and $CO_{2\,(aq)}$. Geochimica et Cosmochimica Acta, 61(3): 501-514.

Hales, B. and Emerson, S., 1997b. Evidence in support of first-order dissolution kinetics of calcite in seawater. Earth and Planetary Science Letters, 148(1): 317-327.

Honjo, S., Manganini, S.J. and Cole, J.J., 1982. Sedimentation of biogenic matter in the deep ocean. Deep Sea Research Part A. Oceanographic Research Papers, 29(5): 609-625.

ILI, 2007. Indiana Limestone Handbook, Indiana Limestone Institute of America, Inc., Belford, IN.

Javadi, K. and Khalili, A., 2009. On generating uniform bottom shear stress. Part II: Shear stress inducing devices. Recent Patents on Chemical Engineering, 2(3): 223-229.

Ji, Y., Baud, P., Vajdova, V. and Wong, T.-f., 2012. Characterization of Pore Geometry of Indiana Limestone in Relation to Mechanical Compaction. Oil & Gas Science and Technology – Revue d’IFP Energies nouvelles, 67(5): 753-775.

Jørgensen, B.B. and Revsbech, N.P., 1985. Diffusive boundary layers and the oxygen uptake of sediments and detritus. Limnology and Oceanography, 30(1): 111-122.

Keir, R.S., 1980. The dissolution kinetics of biogenic calcium carbonates in seawater. Geochimica et Cosmochimica Acta, 44(2): 241-252.

Keir, R.S., 1982. Dissolution of calcite in the deep-sea: theoretical prediction for the case of uniform size particles settling into a well-mixed sediment. American Journal of Science, 282(3): 193-236.

Keir, R.S., 1983. Variation in the carbonate reactivity of deep-sea sediments: determination from flux experiments. Deep Sea Research, 30(3A): 279-296.

Key, R.M., Kozyr, A., Sabine, C.L., Lee, K., Wanninkhof, R., Bullister, J.L., Feely, R.A., Millero, F.J., Mordy, C. and Peng, T.H., 2004. A global ocean carbon climatology: Results from Global Data Analysis Project (GLODAP). Global Biogeochemical Cycles, 18(GB4031).

Khalili, A., Javadi, K., Saidi, A., Goharzadeh, A., Huettel, M. and Jorgensen, B.B., 2008. On Generating Uniform Bottom Shear Stress. Part I: A quantitative study of microcosm chambers. Recent Patents on Chemical Engineering, 1(3): 174-191.

Koutitonsky, V.G. and Bugden, G.L., 1991. The physical oceanography of the Gulf of St. Lawrence: a review with emphasis on the synoptic variability of the motion. In: J.-C. Therriault (Editor), The Gulf of St. Lawrence: small ocean or big estuary? Canadian special publication of fisheries and aquatic sciences, pp. 57-90.

Le Quéré, C., Raupach, M.R., Canadell, J.G., Marland, G., Bopp, L., Ciais, P., Conway, T.J., Doney, S.C., Feely, R.A., Foster, P., Friedlingstein, P., Gurney, K., Houghton, R.A., House, J.I., Huntingford, C., Levy, P.E., Lomas, M.R., Majkut, J., Metzl, N., Ometto, J.P., Peters, G.P., Prentice, I.C., Randerson, J.T., Running, S.W., Sarmiento, J.L., Schuster, U., Sitch, S., Takahashi, T., Viovy, N., van der Werf, G.R. and Woodward, F.I., 2009. Trends in the sources and sinks of carbon dioxide. Nature Geoscience, 2(12): 831-836.

Levich, V.G., 1962. Physicochemical Hydrodynamics. Prentice-Hall International Series in the Physical and Chemical Engineering Sciences. Prentice-Hall Inc., Englewood Cliffs.

Lewis, E. and Wallace, D.W.R., 1998. Program Developed for CO_2 System Calculations. ORNL/CDIAC-105. Carbon Dioxide Information Analysis Center, Oak Ridge National Laboratory, U.S. Department of Energy, Oak Ridge, Tennessee.

Lueker, T.J., Dickson, A.G. and Keeling, C.D., 2000. Ocean $p\mathrm{CO}_2$ calculated from dissolved inorganic carbon, alkalinity, and equations for K_1 and K_2: validation based on laboratory measurements of CO_2 in gas and seawater at equilibrium. Marine Chemistry, 70(1): 105-119.

Lüthi, D., Le Floch, M., Bereiter, B., Blunier, T., Barnola, J.M., Siegenthaler, U., Raynaud, D., Jouzel, J., Fischer, H., Kawamura, K. and Stocker, T.F., 2008. High-resolution carbon dioxide concentration record 650,000-800,000 years before present. Nature, 453(7193): 379-82.

Lüttge, A., 2005. Etch pit coalescence, surface area, and overall mineral dissolution rates. American Mineralogist, 90(11-12): 1776-1783.

Lüttge, A., Arvidson, R.S. and Fischer, C., 2013. A Stochastic Treatment of Crystal Dissolution Kinetics. Elements, 9(3): 183-188.

Millero, F., Huang, F., Zhu, X., Liu, X. and Zhang, J.-Z., 2001. Adsorption and Desorption of Phosphate on Calcite and Aragonite in Seawater. Aquatic Geochemistry, 7(1): 33-56.

Millero, F.J., 1979. The thermodynamics of the carbonic acid system in seawater. Geochimica et Cosmochimica Acta, 43(10): 1651-1661.

Morse, J.W., 1974. Dissolution kinetics of calcium carbonate in seawater: V. Effects of Natural Inhibitors and the Position of the Chemical Lysocline. American Journal of Science, 274: 638-647.

Morse, J.W., 1978. Dissolution kinetics of calcium carbonate in sea water: VI. The near-equilibrium dissolution kinetics of calcium carbonate-rich deep sea sediments. American Journal of Science, 278(3): 344-353.

Morse, J.W. and Arvidson, R.S., 2002. The dissolution kinetics of major sedimentary carbonate minerals. Earth-Science Reviews, 58(1-2): 51-84.

Morse, J.W. and Berner, R.A., 1972. Dissolution kinetics of calcium carbonate in sea water; I, A kinetic origin for the lysocline. American Journal of Science, 272(9): 840-851.

Mucci, A., 1983. The solubility of calcite and aragonite in seawater at various salinities, temperatures and one atmosphere total pressure. American Journal of Science, 283(7): 780-799.

Mucci, A., 1986. Growth kinetics and composition of magnesian calcite overgrowths precipitated from seawater: Quantitative influence of orthophosphate ions. Geochimica et Cosmochimica Acta, 50(10): 2255-2265.

Mucci, A. and Morse, J.W., 1983. The incorporation of Mg^{2+} and Sr^{2+} into calcite overgrowths: influences of growth rate and solution composition. Geochimica et Cosmochimica Acta, 47(2): 217-233.

Mucci, A., Morse, J.W. and Kaminsky, M.S., 1985. Auger spectroscopy analysis of magnesian calcite overgroths precipitated from seawater and solutions of similar composition. American Journal of Science, 285(4): 289-305.

Murphy, J. and Riley, J.P., 1962. A modified single solution method for the determination of phosphate in natural waters. Analytica Chemica Acta, 27: 31-36.

Orr, J.C., Epitalon, J.M. and Gattuso, J.P., 2015. Comparison of ten packages that compute ocean carbonate chemistry. Biogeosciences, 12(5): 1483-1510.

Oxburgh, R., 1998. The Holocene preservation history of equatorial Pacific sediments. Paleoceanography, 13(1): 50-62.

Oxburgh, R. and Broecker, W.S., 1993. Pacific carbonate dissolution revisited. Palaeogeography, Palaeoclimatology. Palaeoecology, 103: 31-39.

Pierrot, D., Lewis, E. and Wallace, D., 2006. MS Excel Program Developed for CO_2 System Calculations. ORNL/CDIAC-105a, Carbon Dioxide Information Analysis Center, Oak Ridge National Laboratory, U.S. Department of Energy, Oak Ridge, Tennessee.

Ridgwell, A. and Hargreaves, J.C., 2007. Regulation of atmospheric CO_2 by deep-sea sediments in an Earth system model. Global Biogeochemical Cycles, 21(GB2008).

Ries, J.B., Ghazaleh, M.N., Connolly, B., Westfield, I. and Castillo, K.D., 2016. Impacts of seawater saturation state (Ω_A = 0.4–4.6) and temperature (10, 25°C) on the dissolution kinetics of whole-shell biogenic carbonates. Geochimica et Cosmochimica Acta, 192: 318-337.

Sabine, C.L. and Feely, R.A., 2007. The oceanic sink for carbon dioxide. In: D. Reay, N. Hewitt, J. Grace and K. Smith (Editors), Greenhouse Gas Sinks. CABI Publishing, Oxfordshire, UK, pp. 31-49.

Santschi, P.H., Bower, P., Nyffeler, U.P., Azevedo, A. and Broecker, W.S., 1983. Estimates of the resistance to chemical transport posed by the deep-sea boundary layer. Limnology and Oceanography, 28(5): 899-912.

Sarmiento, J.L. and Gruber, N., 2006. Ocean Biogeochemical Dynamics. Princeton University Press, Princeton, NJ.

Schink, D. and Guinasso, N., 1977. Modelling the influence of bioturbation and other processes on calcium carbonate dissolution at the sea floor. In: N.R. Andersen and A. Malahoff (Editors), The fate of fossil fuel CO_2 in the oceans. Plenum Press, New York, pp. 375-400.

Schlichting, H., 1979. Boundary Layer Theory. McGraw-Hill, New York.

Sjöberg, E.L., 1978. Kinetics and mechanism of calcite dissolution in aqueous solutions at low temperatures, Stockholm University, Stockholm, 92 pp.

Sjöberg, E.L. and Rickard, D.T., 1984. Calcite dissolution kinetics: Surface speciation and the origin of the variable pH dependence. Chemical Geology, 42(1-4): 119-136.

Steinberger, N. and Hondzo, M., 1999. Diffusional Mass Transfer at Sediment-Water Interface. Journal of Environmental Engineering, 125(2): 192-200.

Subhas, A.V., Rollins, N.E., Berelson, W.M., Dong, S., Erez, J. and Adkins, J.F., 2015. A novel determination of calcite dissolution kinetics in seawater. Geochimica et Cosmochimica Acta, 170: 51-68.

Sun, X. and Turchyn, A.V., 2014. Significant contribution of authigenic carbonate to marine carbon burial. Nature Geoscience, 7(3): 201-204.

Svensson, U. and Dreybrodt, W., 1992. Dissolution kinetics of natural calcite minerals in CO_2-water systems approaching calcite equilibrium. Chemical Geology, 100: 129-145.

Takahashi, T. and Broecker, W.S., 1977. Mechanisms for calcite dissolution on the sea floor. In: N.R. Anderson and A. Malahoff (Editors), The Fate of Fossil Fuel CO_2 in the Oceans Plenum, New York, pp. 455-477.

Tanhua, T., Bates, N.R. and Körtzinger, A., 2013. The Marine Carbon Cycle and Ocean Carbon Inventories. In: G. Siedler, J. Gould and C. J. (Editors), Ocean Circulation and Climate: A 21st Century Perspective. 2nd Ed. International Geophysics, 103. Academic Press, Oxford, GB, pp. 787-815.

Tans, P.P. and Keeling, R., 2016. Dr. Pieter Tans, NOAA/ESRL (www.esrl.noaa.gov/gmd/ccgg/trends/) and Dr. Ralph Keeling, Scripps Institution of Oceanography (scrippsco2.ucsd.edu/).

Teng, H.H., 2004. Controls by saturation state on etch pit formation during calcite dissolution. Geochimica et Cosmochimica Acta, 68(2): 253-262.

Tyrrell, T., 2011. Anthropogenic modification of the oceans. Philosophical Transactions Of The Royal Society, 369(1938): 887-908.

Uppström, L.R., 1974. The boron/chlorinity ratio of deep-sea water from the Pacific Ocean. Deep Sea Research and Oceanographic Abstracts, 21(2): 161-162.

Walter, L.M. and Morse, J.W., 1985. The dissolution kinetics of shallow marine carbonates in seawater: A laboratory study. Geochimica et Cosmochimica Acta, 49(7): 1503-1513.

Williamson, J.H., 1968. Least-squares fitting of a straight line. Canadian Journal of Physics, 46: 1845-1847.

Xu, J., Fan, C. and Teng, H.H., 2012. Calcite dissolution kinetics in view of Gibbs free energy, dislocation density, and pCO_2. Chemical Geology, 322-323: 11-18.

York, D., 1969. Least squares fitting of a straight line with correlated errors. Earth and Planetary Science Letters, 5: 320-324.

York, D., Evensen, N.M., Martínez, M.L. and De Basabe Delgado, J., 2004. Unified equations for the slope, intercept, and standard errors of the best straight line. American Journal of Physics, 72(3): 367.

Zachos, J.C., Röhl, U., Schellenberg, S.A., Sluijs, A., Hodell, D.A., Kelly, D.C., Thomas, E., Nicolo, M., Raffi, I., Lourens, L.J., McCarren, H. and Kroon, D., 2005. Rapid Acidification of the Ocean During the Paleocene-Eocene Thermal Maximum. Science, 308(5728): 1611-1615.

Table 1. Description of dissolution experiments for synthetic sediments with 53 wt% of calcite, with the computed steady-state saturation states with respect to calcite and dissolution rates normalized to the interface surface area (ISA).

stirring speed (rpm)	total sed. mass (g) (± 0.1)	sed. thickness (cm) (± 0.1)	ISA (cm^2) (± 5%)	res. time (hr) (± 0.1)	$\mathrm{pH_T}$ (± 0.003)	TA in (μmol kg^{-1})	TA out (μmol kg^{-1})	Ω_c	ISA-norm. dissolution rate (mol m^{-2} yr^{-1})	[SRP] (μM) (± 0.5%)
0	108.3	2.0	39.6	71.7	7.569	454.6 ± *4.4*	758.3 ± *3.9*	0.64 ± *0.03*	1.4 ± *0.1*	4.3
0	71.9	1.3	39.6	38.5	7.583	520.1 ± *2.5*	696.8 ± *1.9*	0.61 ± *0.02*	1.5 ± *0.1*	0.8
0	62.3	1.6	28.3	22.3	7.506	520.1 ± *2.5*	629.5 ± *0.2*	0.46 ± *0.02*	1.3 ± *0.1*	1.3
0	62.3	1.6	28.3	18.1	7.494	555.0 ± *1.8*	644.6 ± *5.0*	0.47 ± *0.02*	1.3 ± *0.1*	-
0	278.2	5.1	39.6	28.6	7.502	357.2 ± *0.7*	529.6 ± *5.6*	0.38 ± *0.02*	1.1 ± *0.1*	0.8
0	132.8	2.5	38.3	27.9	7.510	575.3 ± *0.2*	810.2 ± *3.0*	0.61 ± *0.03*	1.7 ± *0.1*	0.6
0	132.8	2.5	38.3	27.9	7.555	575.3 ± *0.2*	773.7 ± *3.0*	0.64 ± *0.03*	1.5 ± *0.1*	0.6
0	132.8	2.5	38.3	27.9	7.540	575.3 ± *0.2*	739.2 ± *3.0*	0.59 ± *0.03*	1.2 ± *0.1*	0.6
0	132.8	2.5	38.3	17.3	7.522	585.0 ± *0.8*	660.3 ± *3.0*	0.50 ± *0.02*	0.9 ± *0.1*	0.9
0	132.8	2.5	38.3	17.3	7.522	585.0 ± *0.8*	673.3 ± *3.0*	0.51 ± *0.02*	1.1 ± *0.1*	0.9
0	132.8	2.5	38.3	13.2	7.548	585.0 ± *0.8*	669.6 ± *3.0*	0.54 ± *0.03*	1.3 ± *0.1*	1.1
0	132.8	2.4	38.5	603.1	7.655	581.6 ± *1.5*	913.0 ± *3.0*	0.93 ± *0.04*	0.1 ± *0.0*	2.3
0	132.8	2.4	38.5	384.5	7.644	574.7 ± *2.0*	827.0 ± *3.0*	0.82 ± *0.04*	0.1 ± *0.0*	1.9
0	132.8	2.4	38.5	233.3	7.642	574.7 ± *2.0*	792.0 ± *3.0*	0.78 ± *0.04*	0.2 ± *0.0*	1.4
39	132.4	2.4	39.6	464.9	7.661	581.6 ± *1.5*	943.1 ± *4.7*	0.97 ± *0.05*	0.2 ± *0.0*	2.7
39	132.4	2.4	39.6	296.4	7.647	574.7 ± *2.0*	854.1 ± *4.3*	0.85 ± *0.04*	0.3 ± *0.0*	1.9
39	132.4	2.4	39.6	179.8	7.644	574.7 ± *2.0*	832.8 ± *4.2*	0.82 ± *0.04*	0.4 ± *0.0*	1.4
39	132.4	2.4	39.6	75.5	7.641	574.7 ± *2.0*	982.4 ± *4.9*	0.97 ± *0.05*	1.6 ± *0.1*	1.2
50	132.4	2.4	39.6	66.7	7.636	1045.0 ± *4.2*	1062.4 ± *0.8*	1.05 ± *0.05*	0.1 ± *0.0*	-
74	112.1	2.0	39.6	131.0	7.588	454.6 ± *4.4*	873.0 ± *1.0*	0.77 ± *0.04*	1.0 ± *0.1*	2.3
74	112.1	2.0	39.6	103.1	7.569	454.6 ± *4.4*	874.0 ± *3.0*	0.75 ± *0.04*	1.3 ± *0.1*	2.2
74	115.6	2.1	39.6	74.9	7.592	454.6 ± *4.4*	866.6 ± *8.1*	0.78 ± *0.04*	1.7 ± *0.1*	-
74	115.6	2.1	39.6	66.1	7.593	454.6 ± *4.4*	788.6 ± *4.4*	0.71 ± *0.03*	1.6 ± *0.1*	3.7
74	108.3	2.0	39.6	193.3	7.617	454.6 ± *4.4*	903.1 ± *1.0*	0.85 ± *0.04*	0.7 ± *0.0*	2.6
74	108.3	2.0	39.6	145.3	7.598	454.6 ± *4.4*	866.7 ± *0.5*	0.79 ± *0.04*	0.9 ± *0.1*	-
74	108.2	1.1	72.4	278.7	7.640	454.6 ± *4.4*	933.5 ± *6.9*	0.92 ± *0.04*	0.9 ± *0.0*	2.0
74	108.2	1.1	72.4	196.0	7.623	454.6 ± *4.4*	837.9 ± *3.4*	0.80 ± *0.04*	1.0 ± *0.0*	1.1
74	98.2	1.0	72.4	166.6	7.605	454.6 ± *4.4*	815.3 ± *5.1*	0.74 ± *0.04*	1.1 ± *0.0*	1.4
74	120.7	2.2	39.6	26.3	7.613	520.1 ± *2.5*	730.8 ± *5.4*	0.67 ± *0.03*	2.4 ± *0.1*	0.8
74	98.2	1.0	72.4	79.2	7.666	520.1 ± *2.5*	729.0 ± *0.2*	0.74 ± *0.03*	1.4 ± *0.0*	0.9
74	206.8	3.8	39.6	21.2	7.532	520.1 ± *2.5*	758.3 ± *5.2*	0.59 ± *0.03*	2.7 ± *0.2*	1.6
74	120.7	2.2	39.6	23.4	7.576	555.0 ± *1.8*	746.8 ± *0.9*	0.64 ± *0.03*	2.5 ± *0.1*	-
74	627.9	11.4	39.6	41.6	7.626	357.2 ± *0.7*	736.7 ± *1.2*	0.70 ± *0.03*	3.6 ± *0.2*	2.2
96	108.3	2.0	39.6	89.0	7.577	454.6 ± *4.4*	845.0 ± *4.5*	0.73 ± *0.03*	1.4 ± *0.1*	1.8
96	278.2	5.1	39.6	29.2	7.579	357.2 ± *0.7*	832.9 ± *1.4*	0.72 ± *0.03*	3.0 ± *0.2*	0.8
96	205.8	3.7	39.6	22.6	7.617	357.2 ± *0.7*	690.7 ± *0.3*	0.64 ± *0.03*	3.3 ± *0.2*	0.8
96	205.8	3.7	39.6	22.7	7.585	357.2 ± *0.7*	699.7 ± *2.6*	0.61 ± *0.03*	3.4 ± *0.2*	0.8
96	480.7	8.8	39.6	29.7	7.614	357.2 ± *0.7*	651.1 ± *3.6*	0.60 ± *0.03*	3.2 ± *0.2*	2.0
96	104.9	1.9	39.6	8.8	7.517	397.4 ± *0.5*	553.4 ± *3.5*	0.42 ± *0.02*	6.0 ± *0.3*	6.3
96	97.5	1.8	39.6	10.0	7.532	397.4 ± *0.5*	555.1 ± *2.6*	0.43 ± *0.02*	5.6 ± *0.3*	6.8
96	92.8	1.7	39.6	8.2	7.507	397.4 ± *0.5*	513.6 ± *1.0*	0.37 ± *0.02*	9.3 ± *0.5*	4.7
229	132.4	2.4	39.6	75.8	7.646	989.9 ± *5.5*	1041.3 ± *5.2*	1.04 ± *0.05*	0.2 ± *0.0*	1.2
416	132.4	2.4	39.6	75.8	7.651	982.1 ± *1.1*	1025.7 ± *5.1*	1.04 ± *0.05*	0.2 ± *0.0*	1.2

Table 2. Description of dissolution experiments for synthetic sediments with various calcite contents, with the computed steady-state saturation states with respect to calcite and dissolution rates normalized to the interface surface area (ISA). All dissolution experiments were carried out in unstirred reactors.

calcite dry content (wt%)	total sed. mass (g) (± 0.1)	sed. thickness (cm) (± 0.1)	ISA (cm^2) (± 5%)	res. time (hr) (± 0.1)	pH_T (± 0.003)	TA in (μmol kg^{-1})	TA out (μmol kg^{-1})	Ω_c	ISA-norm. dissolution rate (mol m^{-2} yr^{-1})	[SRP] (μM) (± 0.5%)
10	99.7	2.1	39.6	50.0	7.497	367.5 ± *0.3*	567.5 ± *0.2*	0.41 ± *0.02*	0.5 ± *0.0*	10.7
10	99.7	2.1	39.6	106.6	7.520	367.5 ± *0.3*	662.1 ± *1.0*	0.50 ± *0.01*	0.3 ± *0.0*	13.4
10	99.7	2.1	39.6	502.1	7.652	367.5 ± *0.3*	823.4 ± *2.9*	0.17 ± *0.04*	0.1 ± *0.0*	12.8
70	106.2	2.3	37.4	35.9	7.501	367.5 ± *0.3*	636.2 ± *2.5*	0.46 ± *0.02*	0.9 ± *0.1*	12.7
70	106.2	2.3	37.4	119.3	7.567	367.5 ± *0.3*	722.1 ± *2.1*	0.60 ± *0.03*	0.4 ± *0.0*	13.3
70	106.2	2.3	37.4	465.3	7.648	367.5 ± *0.3*	855.6 ± *3.5*	0.14 ± *0.04*	0.1 ± *0.0*	13.1
90	111.3	1.7	52.8	52.1	7.604	367.5 ± *0.3*	763.5 ± *0.7*	0.71 ± *0.03*	0.7 ± *0.0*	6.8
90	111.3	1.7	52.8	105.5	7.653	367.5 ± *0.3*	793.2 ± *2.6*	0.80 ± *0.04*	0.3 ± *0.0*	7.9
90	111.3	1.7	52.8	410.0	7.665	367.5 ± *0.3*	891.2 ± *3.9*	0.92 ± *0.04*	0.1 ± *0.0*	5.9
100	40.0	0.7	44.2	51.5	7.570	572.3 ± *0.2*	774.1 ± *1.0*	0.67 ± *0.03*	1.0 ± *0.1*	0.4
100	40.0	0.7	44.2	23.8	7.468	572.3 ± *0.2*	676.1 ± *3.0*	0.47 ± *0.02*	1.1 ± *0.1*	0.4
100	40.0	0.7	44.2	23.8	7.525	572.3 ± *0.2*	687.5 ± *0.9*	0.54 ± *0.03*	1.3 ± *0.1*	0.4
100	40.0	0.7	44.2	23.8	7.589	572.3 ± *0.2*	698.9 ± *0.9*	0.63 ± *0.03*	1.4 ± *0.1*	0.7
100	40.0	0.7	44.2	14.7	7.540	585.0 ± *0.8*	649.7 ± *1.9*	0.52 ± *0.02*	1.1 ± *0.1*	0.7
100	40.0	0.7	44.2	14.7	7.522	585.0 ± *0.8*	640.4 ± *1.5*	0.50 ± *0.02*	1.0 ± *0.0*	0.9
100	40.0	0.7	44.2	11.7	7.550	585.0 ± *0.8*	656.9 ± *1.1*	0.54 ± *0.03*	1.6 ± *0.1*	0.9
100	96.4	1.5	52.8	512.3	7.671	367.5 ± *0.3*	902.1 ± *2.4*	0.95 ± *0.04*	0.1 ± *0.0*	1.0

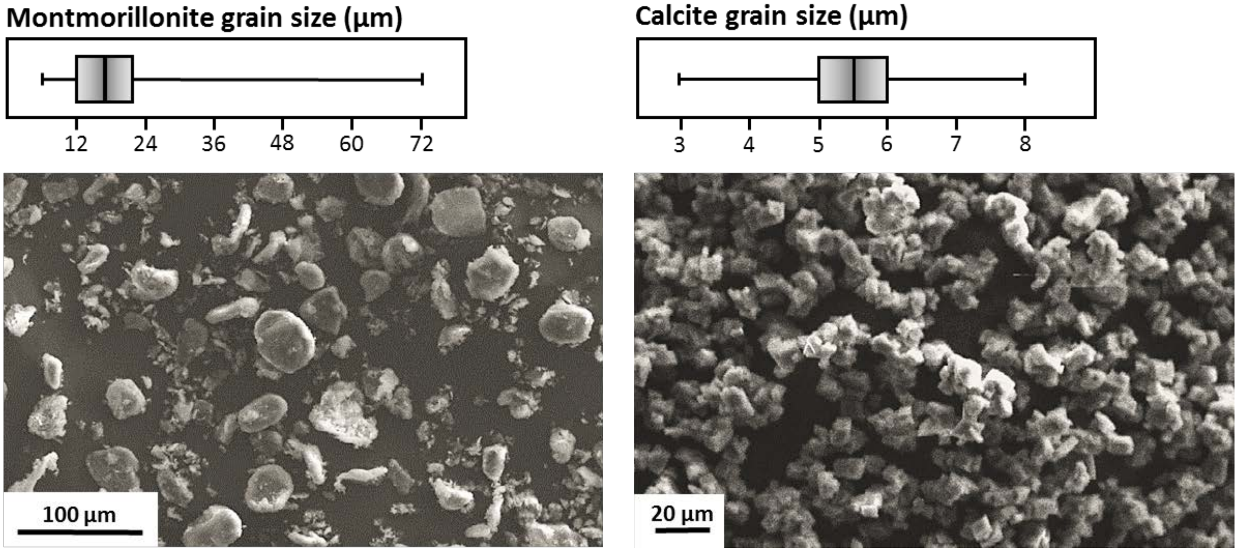

Fig. 1. Scanning electron microscope image of (left) montmorillonite and (right) calcite powder. Boxplots represent the distribution of grain size (diameter expressed in µm) of the montmorillonite powder for a sample of 100 grains, and of calcite powder for a sample of 150 grains. Each boxplot depicts the minimum and maximum measured grain sizes, the median value, and the first and third quartiles.

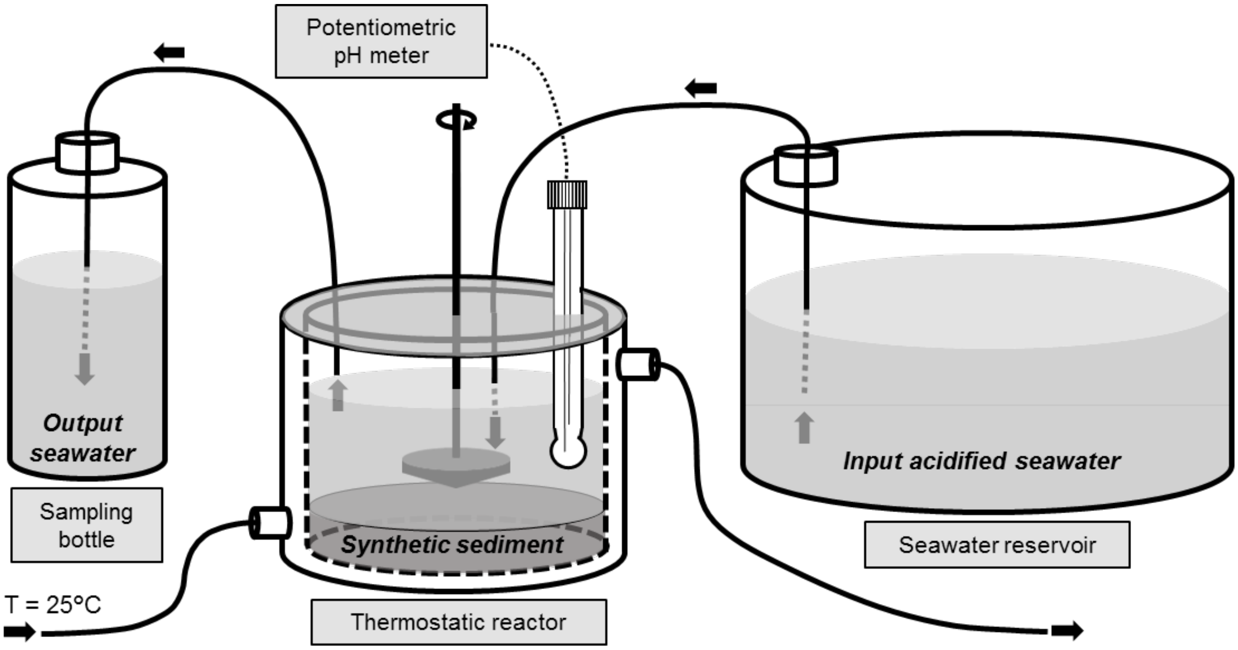

Fig. 2. Schematic representation of the experimental design.

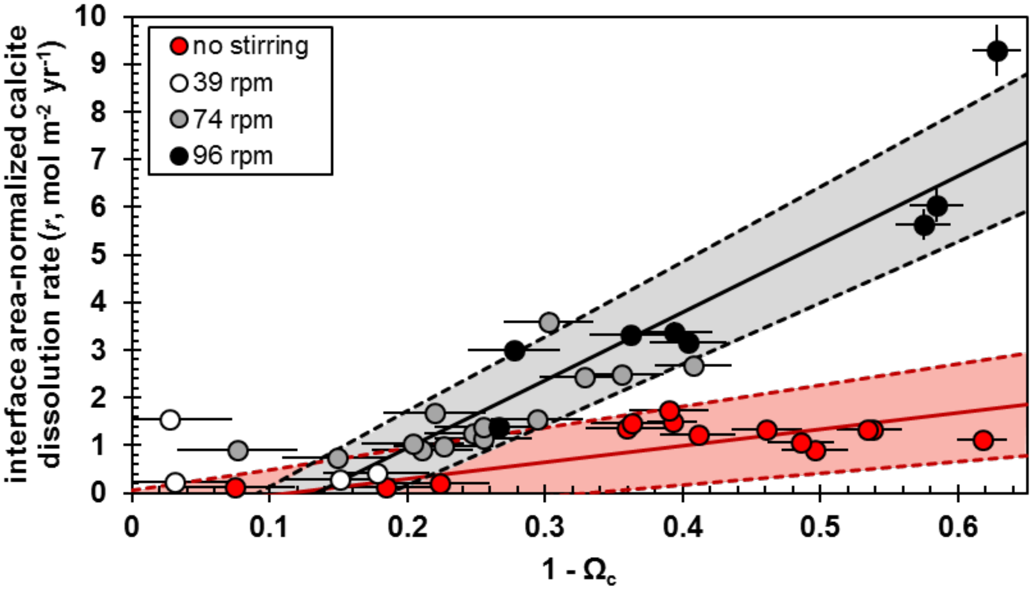

Fig. 3. Steady-state ISA-normalized calcite dissolution rate as a function of the steady-state undersaturation state ($1 - \Omega_c$). The color of each point represents the stirring speed used during the dissolution experiments. Uncertainties are represented by error bars on both the saturation state and the dissolution rate. The red and the black solid lines are, respectively, the linear bivariate fit to the experimental dissolution data obtained in unstirred (Eq. (7a)) and stirred reactors (Eq. (8b)), and the dashed lines describe the standard errors for each model.

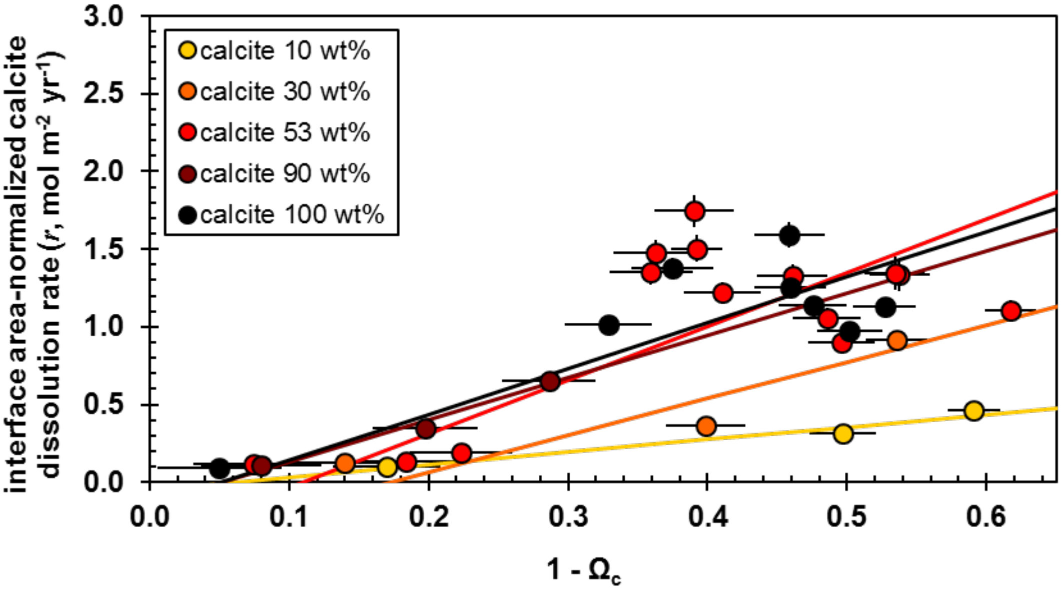

Fig. 4. ISA-normalized calcite dissolution rates as a function of the undersaturation state. The color of the data points represents the calcite content and the solid lines are the linear bivariate fits for each of the calcite contents.

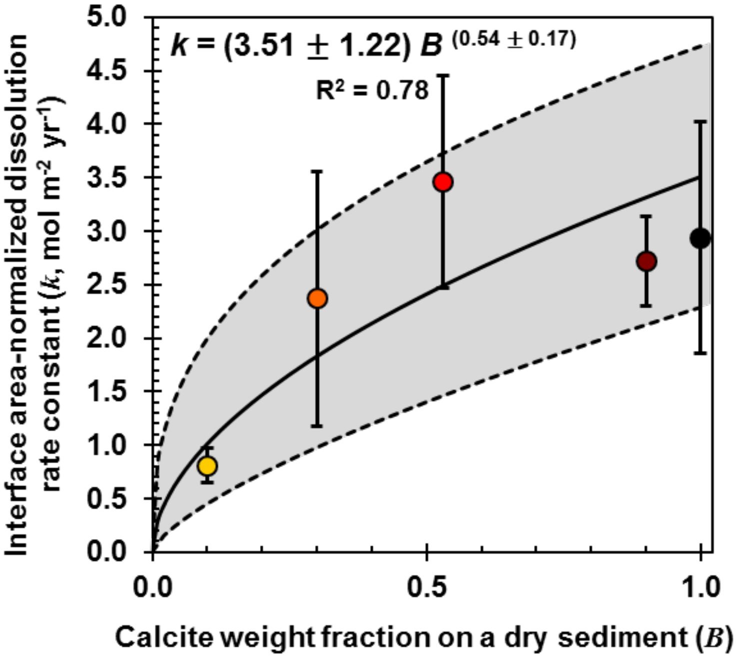

Fig. 5. The apparent ISA-normalized rate constants (*k*, with error bars) as a function of the calcite content (*B*) of the sediment disks. The solid line is a standard power regression model (equation given in the graph) and the dashed lines represents its uncertainties.

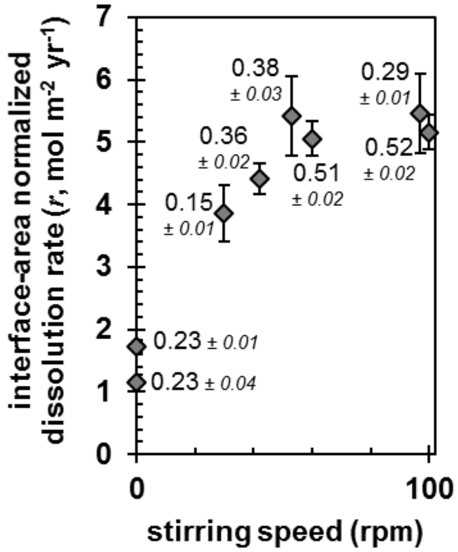

Fig. 6. Indiana limestone calcite dissolution rates as a function of the stirring speed. The labels indicate the measured steady-state saturation state with respect to calcite (Ω_c) in the bulk seawater for each experiment.

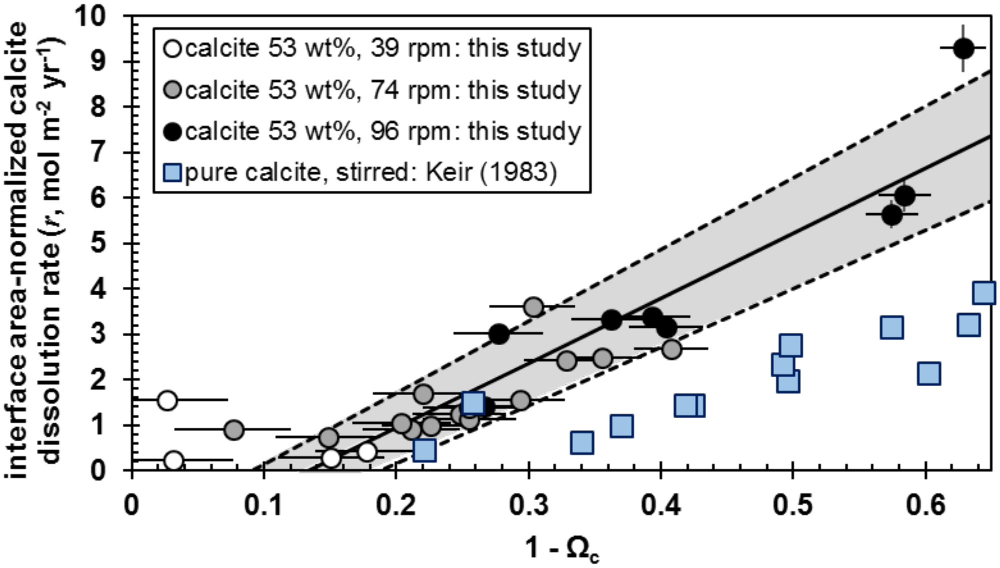

Fig. 7. Comparison of the dissolution rates measured by Keir (1983) in a stirred reactor on pure synthetic calcite with our experimental data on the dissolution rates of synthetic sediments (53 wt% of calcite at various stirring rates) as a function of the steady-state undersaturation state.